Kinetic modelling of the role of the aldehyde dehydrogenase enzyme and the breast cancer resistance protein in drug resistance and transport

M.I. Atari [a,*], M.J. Chappell [a], R.J. Errington [b], P.J. Smith [c], N.D. Evans [a]

[a] School of Engineering, University of Warwick, Coventry CV4 7AL, UK

[b] Department of Medical Biochemistry and Immunology, University of Wales College of Medicine, Cardiff University, Cardiff CF14 4XN, UK

[c] Department of Pathology, University of Wales College of Medicine, Cardiff University, Cardiff CF14 4XN, UK

Abstract: A compartmental model for the *in vitro* uptake kinetics of the anti-cancer agent topotecan (TPT) has been extended from a previously published model. The extended model describes the drug activity and delivery of the pharmacologically active form to the DNA target as well as the catalysis of the aldehyde dehydrogenase (ALDH) enzyme and the elimination of drug from the cytoplasm via the efflux pump. Verification of the proposed model is achieved using scanning-laser microscopy data from live human breast cancer cells. Before estimating the unknown model parameters from the experimental *in vitro* data it is essential to determine parameter uniqueness (or otherwise) from this imposed output structure. This is formally performed as a structural identifiability analysis, which demonstrates that all of the unknown model parameters are uniquely determined by the output structure corresponding to the experiment.

Keywords: efflux pump; drug kinetics; topotecan; aldehyde dehydrogenase; structural identifiability; parameter estimation.

[*] Corresponding author. Tel: +44 2476 572904; fax: +44 2476 418922.

E-mail address: M.I.Atari@warwick.ac.uk (M.I. Atari)

1. Introduction

This paper presents a novel extension of a non-linear drug kinetic model, by Evans et al.[1], on the *in vitro* uptake of the anti-cancer agent topotecan (TPT) for live human breast cancer cells (MCF-7 cell line) in order to account for cell transporters and drug resistance proteins. In this paper, the transporter located in the cell membrane acts as an efflux pump to drive the drug out of the cell before it can reach the target in the nucleus. The model permits analysis of the kinetics and temporal interactions of the pharmacologically active form of the drug to the DNA target. The scanning-laser microscopy experiment used to collect the data imposes an output structure on the model that corresponds to the functions of the variables that can be directly observed or measured (in this case, total concentrations of TPT in extracellular medium, cytoplasm and nucleus).

This paper consists of five main sections, including the introduction (Section 1), Section 2 provides a background on the underlying biochemistry of the anti-cancer agent TPT in addition to an introduction to drug efflux pumping mechanism and resistance proteins. Section 3 includes a detailed explanation of the mathematical model developed and a reduced order model generated via quasi-steady state assumptions that also yields a reduction in the number of the unknown model parameters.

The symbolic software MATHEMATICA [2] was used in this study to perform a structural identifiability analysis of the model (Section 4). Finally, experimental data collected have been used for parameter estimation (Section 5) using the software package FACSIMILE (MCPA Software, U.K.), further results and concluding remarks are outlined in this section.

2. Background

2.1 Action of the anti-cancer agent TPT

TPT is a derivative of Camptothecin (CPT), an extract from the Chinese tree *Camptotheca acuminata* and is water-soluble [3-5]. CPT is specific in that it acts as a reversible poison of the DNA cellular enzyme topoisomerase I [6]. TPT has been widely used against ovarian and small cell lung carcinomas [1]. The function of topoisomerase I enzyme is to facilitate DNA supercoiling by cleavage and

religation of one strand of double-stranded DNA (dsDNA) [7]. Topoisomerase I is targeted by TPT in the nucleus, and traps it in a reversible ternary complex with DNA. The death of TPT-targeted cells results from the collision between the complex and the DNA replication process causing the dsDNA to break resulting in cell death [4,6].

The ring-closed, parent lactone form (TPT-L) undergoes reversible hydrolysis to an open-ringed hydroxy acid form (TPT-H). TPT-L is the pharmacologically active form in that it is the form of TPT which is responsible for inhibiting the enzyme topoisomerase I reversibly and maintaining the TPT-topoisomerase I-DNA complex as well as DNA binding. The reversible hydrolysis process is pH dependent, in which the parent form predominates at a high-acidic medium pH (<4), whereas the hydroxy acid form prevails in a high-basic medium pH (>10) [8-9].

The reversible hydrolysis of TPT-L was modelled by Evans et al. [10] using a linear two-compartment model with parameter estimation from high performance liquid chromatography (HPLC) data in buffers at different pH levels. A non-linear five-compartment model describing the uptake kinetics of TPT in a medium enclosing human lymphoma cells (SU-DHL-4 cell line) was developed based on the two-compartment model. The non-linear model characterises the kinetics of TPT in the entire cell population [1]. Similar to the model in Evans et al. [10], the unknown parameters for the five-compartment model were estimated from HPLC data.

TPT is a naturally fluorescent agent which can be excited using ultra-violet wavelengths (350-360 nm) and detected at a visible wavelength with peak emission at 540 nm. Accordingly, HPLC is used to compute the amount of drug in human plasma [10] and extracts. The binding characteristics of drug to DNA have been determined using the high-photon absorption property [8]. In the current paper, delivery and localisation of the drug in single cells are examined using two-photon laser scanning microscopy. The optical sectioning capacity of this technique provides high-resolution spatial information representing the fluorescence intensity in the compartments and, therefore, quantifying the drug concentration in these compartments, i.e. nucleus, cytoplasm and extra-cellular environment. The kinetics of the uptake for each sub-compartment can be analysed via time-lapse sequences, thus providing the primary data for mathematical modelling, and parameter estimation.

2.2 The BCRP/ABCG2 drug efflux pump and the enzyme ALDH

One of the major forms of cancer treatment is chemotherapy. In general, cancers are either resistant to chemotherapy or obtain resistance during treatment, thereby leading to ineffective chemotherapy [11]. Examples of drugs to which resistance has been observed or acquire resistance during treatment include topoisomerase inhibitors (eg, TPT), anthracyclines (eg, doxorubicin), the *Vinca* alkaloids (eg, vincristine) and the taxanes (eg, paclitaxel) [11]. The model in this paper describes the mechanism by which human cancers develop resistance to drugs, that is, the overexpression of efflux transport proteins in the plasma membrane of cancer cells. Examples include, P-glycoprotein (P-gp) [12] in addition to the multidrug resistance protein 1 (MRP1) [13]. More recently, other human binding cassette (ABC) transporters that are involved in the resistance of anti-cancer drugs have been discovered. The most important of these is the breast cancer resistance protein (BCRP) also known as ABCG2 [14], placenta specific ABC protein [15] or mitoxantrone-resistance protein [16].

Studies conducted in various laboratories have verified that enforced expression of BCRP complementary DNA in different types of cells caused resistance to multiple anti-cancer drugs including TPT and reduced drug accumulation in the cell [17-19]. This protein is significantly expressed in organs central for absorption, distribution, elimination, and deposition of drugs. Further investigations have come to the conclusion that BCRP plays a significant role in drug deposition [11]. BCRP, also known as ABCG2, is the second member of the sub-family G of the human ATP binding cassette (ABC) transporter. Moreover, BCRP is a half-transporter, in that it consists of a one nucleotide binding domain followed by a one membrane-spanning domain, which is unlike P-gp and MRP1 which are arranged in two repeated halves. It has been shown from various studies on drug efflux mechanisms that BCRP is mostly localised at the plasma membrane instead of at internal vesicular membranes. Therefore, BCRP is presumably in active transport from the cell rather than in transport into internal vesicles [14,20-21]. The actual efflux pumping mechanism is explained in detail in the following section.

Aldehyde dehydrogenases (ALDHs) [aldehyde: $NAD(P)^+$ oxidoreductase] are an enzyme group that catalyse the conversion of aldehydes to the corresponding acids irreversibly by means of an $NAD(P)^+$-dependent reaction [22]. ALDHs are distinguished based on properties including physicochemical

characteristics, enzymological, subcellular localisation and tissue distribution [23]. ALDH enzymes demonstrate high activity in oxidising aldophosphamide and detoxifying anti-cancer agents. It has been proven that this drug resistance was associated with the transcriptional activation of ALDH expression in cancer cells [24].

3 Mathematical model

3.1 Extended model

The original model proposed by Evans et al. [1] allows for mixing in the medium by dividing the medium into two separate pools: the medium region into which the drug is added and the extracellular region in which the cells are located. The drug exchange between the cells and medium takes place only through the extracellular region. In this model, the cellular pool that contains all of the individual cells has been extended to include the cell membrane. Therefore, this leads to a model with five experimental regions: the medium, the extracellular region, the cell membrane, the cytoplasm, and the nucleus which are denoted by subscripts *m*, *e*, *cm*, *c*, and *n*, respectively.

Fig. 1 provides a schematic diagram of the extended compartmental model, where L and H stand for the concentrations of TPT-L and TPT-H, respectively. Therefore, $L_m(t)$, $L_e(t)$, $L_c(t)$, and $L_n(t)$, denote the concentrations of TPT-L in the medium, extracellular region, cytoplasm and nucleus respectively, at time t following the addition of drug. The corresponding variables for TPT-H are $H_m(t)$, $H_e(t)$, and $H_c(t)$. The concentration of TPT-H bound to the efflux pump is denoted by $TH_{cm}(t)$, and the variable $T(t)$ represents the total concentration of available ABCG2 (drug transporter) binding sites at time t. TPT-H (the form favoured by the efflux pump) in the cytoplasm (H_c) binds to the drug transporter (T) to form an intermediate complex (TH_{cm}) which breaks in one way to release free drug transporter (T_0) and TPT-H in the extracellular region (H_e). In Evans et al. [1,10], it is assumed that all drug in the nucleus is bound and only TPT-L binds to DNA. This assumption is a simplification of the real case in which the nucleus may contain unbound drug as well; therefore, this postulation requires further experimental investigation. In the three experimental pools, i.e. medium, extracellular region and cytoplasm, TPT undergoes reversible and pH dependent hydrolysis. Assuming homogeneity in pH

and/or any other factors that might have an effect on the hydrolysis, the rate constants are k_{cm} and k_{om} for the ring closing of TPT-H and ring opening of TPT-L, respectively, for both the medium and the extracellular region. Additionally, the corresponding rate constants for the cytoplasm are k_{cc} and k_{oc}. ALDH isozymes including ALDH1A1, are important for multiple biological activities including drug resistance [25-26]. We have demonstrated that the uptake of TPT in cells exposed to an ALDH inhibitor (disulfiram) is enhanced (unpublished; data not shown). Moreover, kinetic analysis of TPT uptake also suggests that the change in charge upon ring hydrolysis would favour exclusion via the ABCG2 pump, and this is the overriding process to remove TPT from the cellular environment [27]. Therefore based on these analyses, the active drug in the cytoplasm is assumed to bind irreversibly to the enzyme ALDH where it is converted to the form favoured by the efflux pump (TPT-H). The rate at which TPT-L binds to ALDH is assumed to be proportional, with the association rate k_a, to the product of the concentrations of TPT-L in the cytoplasm, $L_c(t)$, and free enzyme, $E(t)$. Additionally, dissociation of drug bound to ALDH occurs at a first-order rate, with rate constant k_d. If E_0 denotes the total concentration of available ALDH, then the concentration of free ALDH is $E(t) = E_0 - EL_c(t)$, where $EL_c(t)$ is the concentration of enzyme-drug complex. In the nucleus, it is assumed that only TPT-L binds to DNA and that all drug is bound.

(**Fig. 1 here**)

Mixing between the medium and extracellular pools can be modelled by first-order flows between them. Assuming that the rate constants are the same for the lactone and hydroxy acid forms, k_{mi} denotes the flow from the medium to the extracellular pool and k_{mo} denotes the flow out of the extracellular pool to the medium.

Flow between the extracellular region and the cellular pool, including the cell membrane and cytoplasm, takes place simultaneously via two distinct processes. The first process is the efflux pumping mechanism in which the BCRP/ABCG2 transporter carries TPT-H through the cell membrane to the extracellular region irreversibly. The rate at which TPT-H in the cytoplasm binds to

the efflux pump is assumed to be proportional, with association rate constant k_1, to the product of the concentrations of the inactive drug in the cytoplasm, $H_c(t)$, and free transporter, $T(t)$. The dissociation of drug bound to the efflux pump (TH_{cm}) is assumed to be first order with rate constant k_2. If T_0 denotes the total concentration of available (BCRP/ABCG2) drug transporter, then the concentration of free transporter is the difference between T_0 and the concentration of bound drug (TH_{cm}), that is $T(t) = T_0 - TH_{cm}(t)$. The second is the diffusion between the cytoplasm and the extracellular region, which is modelled via a first-order process. Note however, that only TPT-L diffuses across the cell membrane, based on previous observations and physical properties of TPT-H with respect to the lipid bilayer traverse. The rate constant for influx of $L_e(t)$ into the cytoplasm is k_i and the rate constant for the efflux of $L_c(t)$ into the extracellular pool is k_e. Similarly, the binding rate of TPT-L to DNA is assumed to be proportional (with constant k_b) to the product of the concentrations of TPT-L in the cytoplasm and free binding sites $B_F(t)$. Let B_T denote the total concentration of available DNA binding sites, therefore, the concentration of free sites, $B_F(t)$, is the difference between B_T and the concentration of bound drug, $L_n(t)$, that is $B_F(t) = B_T - L_n(t)$. Dissociation of bound drug is assumed to occur at a first-order rate as either TPT-L, with rate constant k_{dl}, or TPT-H, with rate constant k_{dh}. Thus TPT-L may bind to DNA in a reversible manner and can then, once bound, be converted to TPT-H [28].

If the volumes of the medium, extracellular region, cytoplasm, cell membrane and nucleus, are denoted by V_m, V_e, V_c, V_{cm}, and V_n, respectively, then the postulated mathematical model for the uptake kinetics of TPT is given by the following system of differential equations:

$$\frac{dL_m}{dt} = -(k_{om} + k_{mi})L_m + k_{cm}H_m + k_{mo}v_0L_e \tag{1}$$

$$\frac{dH_m}{dt} = k_{om}L_m - (k_{cm} + k_{mi})H_m + k_{mo}v_0H_e \tag{2}$$

$$\frac{dL_e}{dt} = \frac{k_{mi}L_m}{v_0} - (k_{mo} + k_{om} + k_i)L_e + k_{cm}H_e + \frac{k_eL_c}{v_1} \tag{3}$$

$$\frac{dH_e}{dt} = \frac{k_{mi}H_m}{v_0} + k_{om}L_e - (k_{cm} + k_{mo})H_e + \frac{v_3k_2TH_{cm}}{v_1} \tag{4}$$

$$\frac{dL_c}{dt} = k_iv_1L_e - (k_e + k_{oc})L_c + k_{cc}H_c + k_{dl}v_2L_n - k_b(B_T - L_n)L_c - k_a(E_0 - EL_c) \tag{5}$$

$$\frac{dH_c}{dt} = k_{oc}L_c - k_{cc}H_c + k_{dh}v_2L_n - k_1(T_0 - TH_{cm})H_c + k_d EL_c \quad (6)$$

$$\frac{dL_n}{dt} = \frac{k_b}{v_2}(B_T - L_n)L_c - (k_{dl} + k_{dh})L_n \quad (7)$$

$$\frac{dTH_{cm}}{dt} = \frac{k_1H_c(T_0 - TH_{cm})}{v_3} - k_2TH_{cm} \quad (8)$$

$$\frac{dEL_c}{dt} = k_aL_c(E_0 - EL_c) - k_dEL_c \quad (9)$$

where, $v_0 = V_e/V_m$, $v_1 = V_e/V_c$, $v_2 = V_n/V_c$, $v_3 = V_{cm}/V_c$, and $v_1/v_3 = V_e/V_{cm}$. Time $t = 0$ corresponds to the (first) addition of drug as a bolus injection. The corresponding initial conditions for the model are given by:

$$H_m(0) = L_e(0) = H_e(0) = L_c(0) = H_c(0) = L_n(0) = EL_c(0) = TH_{cm}(0) = 0, \text{ and } L_m(0) = (1 + v_0)D, \quad (10)$$

where D is the concentration of dose in the full physical medium (i.e. 2 ml or 2×10^{12} μm^3).

According to Evans et al. [1,10], the estimates obtained for the volumes, using data collected from optical sectioning using a confocal microscope, are: $V_c + V_{cm} = 829$ μm^3 (SD=232 μm^3) for the average volume of cytoplasm and cell membrane in single cell; the volume of the nucleus in a single cell (V_n) is 326 μm^3 (SD=85.5 μm^3); and therefore, the total volume of the average cell ($V_c + V_{cm} + V_n$) is 1155 μm^3. According to the above values, the radius of the cell can be calculated assuming that the cell is spherical, therefore, the average radius of a single cell is 6.51 μm and the average radius of the nucleus in a single cell is 4.27 μm. The cell membrane thickness is approximately 3-10 nm [29]. There is therefore relatively little variation in the plasma membrane thickness between cells. In this model, the chosen value of the membrane thickness is 7 nm. The resulting calculations for the average volumes of V_{cm}, and V_c in a single cell are 8.4 μm^3 and 820.5 μm^3, respectively. The culture medium has a volume of 2×10^{12} μm^3, therefore:

$V_m + V_e = 2\times10^{12}$ μm^3,
and so,
$V_e = \frac{2\times10^{12}v_0}{1+v_0}$ μm^3.

Given that the culture medium contains 1×10^5 cells, the cellular volume ratios are given by:

$$v_1 = \frac{V_e}{V_c} = \left(\frac{v_0}{1+v_0}\right)\left(\frac{2\times10^{12}}{(1+10^5)\times820.5}\right) = \frac{\alpha v_0}{1+v_0}$$

where $\alpha = 2.4375\times10^4$, $v_2 = 3.9732\times10^{-1}$, and $v_3 = 1.0238\times10^{-2}$. Evans et al. [10] used experimental data for the hydrolysis of TPT in buffers with different pH to obtain values for the ring opening and closing rate constants against pH. Cells were placed in a medium with pH = 7.2 in the experiments used to collect data for estimating unknown parameters in the proposed model. With the assumption that the hydrolysis rate constants are primarily dependent on pH the corresponding values for k_{om}, k_{cm}, k_{oc} and k_{cc} from Evans et al. [1,30] are used, these values are $k_{om} = k_{oc} = 1.5599\times10^{-4}$ s^{-1} and $k_{cm} = k_{cc} = 2.9553\times10^{-4}$ s^{-1}. In the experiment used to collect data for parameter estimation, concentrations were measured in μM, the initial dose was $D = 10$ μM, and time was measured in seconds.

3.2 Pseudo-steady state approximation of the model

In this section, the extended model in Fig. 1 is reduced by assuming that the binding kinetics of both the ALDH enzyme and the BCRP/ABCG2 efflux pump are saturable within the physical volume of space considered. That is the concentrations of the enzyme and the transporter are much lower than the concentration of associated substrates. A structural identifiability analysis (Section 4) of the unknown parameters of the system is performed for the reduced system following a pseudo-steady state approximation [30]. The structural identifiability properties of the reduced model will change from those of the original system [31]. Therefore, fewer system parameters (of the basic model) may be structurally globally identifiable as they enter in new parameter groupings in the reduced order model. This technique is widely applied to models in pharmacokinetics, biology and biomedicine.

The assumptions on the relative sizes of the model parameters, are the following, firstly, the concentration of the enzyme is much lower than the active form of the drug in the cytoplasm, that is $E_0 << L_c$ and/or the binding affinity of the enzyme ALDH is much lower than unity, $k_d/k_a << 1$. Secondly, the concentration of the transporter (BCRP/ABCG2) is much lower than the concentration of the inactive form of the drug in the cytoplasm, $T_0 << H_c$ and/or the binding affinity of the transporter

is low $k_2/k_1 << 1$. Following the administration of drug, saturation of the available binding sites (enzyme and transporter) or equilibrium of bound substances is virtually instantaneous, whereby a quasi-steady state approximation can be made [31].

According to the assumptions above, the intermediate compounds TH_{cm} and EL_c reach an equilibrium state rapidly and therefore, (8) and (9) have zero rate of change. Therefore (4), (5), and (6) can be reformulated and reduced to (11), (12), and (13) respectively:

$$\frac{dH_e}{dt} = \frac{k_{mi}}{v_0} H_m + k_{om} L_e - (k_{cm} + k_{mo}) H_e + \frac{v_3 V_{m1} H_c}{v_1 (v_3 k_{m1} + H_c)} \tag{11}$$

$$\frac{dL_c}{dt} = k_i v_1 L_e - (k_e + k_{oc}) L_c + k_{cc} H_c + k_{dl} v_2 L_n - k_b (B_T - L_n) L_c - \frac{V_{m2} L_c}{(k_{m2} + L_c)} \tag{12}$$

$$\frac{dH_c}{dt} = k_{oc} L_c - k_{cc} H_c + k_{dh} v_2 L_n - \frac{v_3 V_{m1} H_c}{(v_3 k_{m1} + H_c)} + \frac{V_{m2} L_c}{(k_{m2} + L_c)} \tag{13}$$

where $k_{m1} = k_2/k_1$, $k_{m2} = k_d/k_a$, $V_{m1} = k_2 T_0$ and $V_{m2} = k_a E_0$. The k_{mi} values represent Michaelis-Menten constants and V_{mi} values are the numerical constants that represent the maximum velocity obtained when the enzyme and the transporter exist completely in the form TH_c (i = 1) and EL_c (i = 2), respectively [32].

Such (outer solution) approximations provide accurate results for the asymptotic behaviour of drug uptake. Moreover, the number of unknown parameters in the model has been reduced by two and the system equations are reduced to seven.

4. Identifiability analysis

4.1 Structural identifiability

Based on the microscopy experiments used to collect data for parameter estimation, an output structure on the suggested model has been imposed. This consists of functions of the model variables that are directly measured. The output structure has to uniquely determine the unknown parameters in the postulated model to obtain meaningful parameter estimates. If the unknown parameters are not uniquely determined, the proposed experiment should be redesigned (if possible) in order to obtain an

output structure that uniquely determines the unknown parameters. Therefore, a structural identifiability analysis is a prerequisite for experiment design, system identification and parameter estimation. In mathematical terms, consider a postulated parametric model given by:

$$\dot{\mathbf{x}}(t,\mathbf{p}) = \mathbf{f}(\mathbf{x}(t,\mathbf{p}),\mathbf{p}) \tag{14}$$

$$\mathbf{x}(0,\mathbf{p}) = \mathbf{x}_0(\mathbf{p}) \tag{15}$$

$$\mathbf{y}(t,\mathbf{p}) = \mathbf{h}(\mathbf{x}(t,\mathbf{p}),\mathbf{p}) \tag{16}$$

where $\mathbf{p} = (p_1, \ldots, p_q)^{\mathrm{T}}$ is a constant q-dimensional vector representing the unknown model parameters and lies in some open set $\Omega \subset \mathbb{R}^q$ of feasible vectors. It is assumed that both $\mathbf{f}(\cdot, \mathbf{p})$ and $\mathbf{h}(\cdot, \mathbf{p})$ are fractions of polynomials (i.e., rational functions) in both $\mathbf{x}$ and $\mathbf{p}$. The n-dimensional vector $\mathbf{x}(t, \mathbf{p}) = (x_1(t, \mathbf{p}), \ldots, x_n(t, \mathbf{p}))^{\mathrm{T}}$ is the state vector, where $x_i(t, \mathbf{p})$ are the model variables. $M(\mathbf{p})$ is a connected open subset of $\mathbb{R}^n$ such that $\mathbf{x}(t,\mathbf{p}) \in \mathrm{M}(\mathbf{p})$ for all $t \geq 0$. The vector $\mathbf{y}(t, \mathbf{p}) = (y_1(t, \mathbf{p}), \ldots, y_r(t, \mathbf{p}))^{\mathrm{T}}$ is the response function or the observation function, where $\mathbf{y}(t,\mathbf{p}) \in \mathbb{R}^r$. It is also assumed that the initial condition $\mathbf{x}_0(\cdot)$ is a fraction of polynomials in $\mathbf{p}$.

According to the proposed experiment, r linear combinations of the variables of the model are measured, $c_{i1}(\mathbf{p})x_1(t, \mathbf{p}) + \cdots + c_{in}(\mathbf{p})x_n(t, \mathbf{p})$, $(i = 1, \ldots, r)$. Thus the following equation represents the output structure of the model for the systems considered:

$$\mathbf{y}(t,\mathbf{p}) = \mathbf{C}(\mathbf{p})\mathbf{x}(t,\mathbf{p}) \quad \text{where} \quad \mathbf{C}(\mathbf{p}) = \begin{pmatrix} c_{11}(\mathbf{p}) & \cdots & c_{1n}(\mathbf{p}) \\ \vdots & & \vdots \\ c_{r1}(\mathbf{p}) & \cdots & c_{rn}(\mathbf{p}) \end{pmatrix}. \tag{17}$$

The input in this particular experiment consists of a single impulse, i.e. injection of the drug TPT into the system, therefore, the corresponding amounts, are included in the initial conditions $\mathbf{x}_0(\mathbf{p})$. Otherwise, there are no external inputs to the system and no further input terms are included in (14).

If a parameter can take any of a distinct (countable) number of values for a given observation function, $\mathbf{y}(t, \mathbf{p})$, then the parameter is locally identifiable [33]. In particular, if the parameter can only take a unique value (in the entire parameter space) for the given observation function, then the parameter is globally (uniquely) identifiable for that particular experiment. Otherwise, the parameter is unidentifiable.

Definition 1. A compartmental system of the form (14) – (17) is said to be *structurally globally/uniquely identifiable* if all the unknown parameters of the model are globally/uniquely identifiable.

Definition 2. A compartmental model of the form (14) – (17) is said to be *structurally locally identifiable* if all the unknown parameters of the model are locally identifiable and at least one parameter (p_i) is not globally identifiable.

Definition 3. Otherwise, a model of the form (14) – (17) is said to be *unidentifiable* if at least one of the unknown parameters (p_i) of the model is unidentifiable.

The Taylor series approach [34] is applicable to systems in which the administration is through bolus injection. This method depends upon expanding components of $\mathbf{y}(t, \mathbf{p})$, the observation function, as Taylor series around $t = 0^+$. An important condition to perform this test is that the observation must be analytic. For the system described in (14) – (17), the Taylor series approach is used to verify that the system is structurally globally identifiable. Uniqueness of the coefficients in the Taylor series expansions of $y_i(t, \mathbf{p})$ entails the following, if $\bar{\mathbf{p}} \in \boldsymbol{\Omega}$ is such that $\mathbf{y}(t, \mathbf{p}) = \mathbf{y}(t, \bar{\mathbf{p}})$ for all $t \geq 0$, then, for each $i = 1, \ldots, r$ and $k = 1, 2, 3, \ldots$

$$y_i^{(k)}(0,\mathbf{p}) = y_i^{(k)}(0,\bar{\mathbf{p}}) \text{ where, } y_i^{(0)}(0,\mathbf{p}) = y_i(0,\mathbf{p}). \tag{18}$$

4.2 Structural identifiability analysis of the system

For the structural identifiability analysis of this model, the Taylor series approach is applied to the pseudo-steady state model ((1)-(3) and (7)-(13)) with initial conditions given in (10). The vector $\mathbf{p}$ comprising the thirteen unknown parameters of the model is given by:

$$\mathbf{p} = (k_{mi}, k_{mo}, k_i, k_e, k_b, k_{dl}, k_{dh}, B_T, v_0, V_{m1}, k_{m1}, V_{m2}, k_{m2})^{\mathsf{T}}.$$

The model parameters are positive, therefore, the set of feasible parameter vectors, Ω, comprises the vectors $(p_1, \ldots, p_{11})^{\mathsf{T}}$ such that $p_i > 0$ $(1 \leq i \leq 13)$. The set $M(\mathbf{p})$ is $\square^7$ and the initial condition for the state space representation of the model (for $D = 10$ μM) is given by:

$$\mathbf{x}_0(t,\ \mathbf{p}) = ((1+v_0)D, 0, 0, 0, 0, 0, 0)^{\mathsf{T}}$$

An arbitrary parameter vector is denoted by $\bar{\mathbf{p}}$ such that:

$$\bar{\mathbf{p}} = (\bar{k}_{mi}, \bar{k}_{mo}, \bar{k}_i, \bar{k}_e, \bar{k}_b, \bar{k}_{dl}, \bar{k}_{dh}, \bar{B}_T, \bar{v}_0, \bar{V}_{m1}, \bar{k}_{m1}, \bar{V}_{m2}, \bar{k}_{m2})^{\mathsf{T}}$$

for which, $\mathbf{y}(t,\ \mathbf{p}) = \mathbf{y}(t,\ \bar{\mathbf{p}})$ for all $t \geq 0$. Computer algebra systems such as MATHEMATICA have proven helpful for the symbolic calculation of these coefficients, particularly when they become algebraically complicated. For $k = 0$ in (18) for $i = 1$, 2 and 3, yields no information since each of these coefficients is 0. For $k = 1$ in (18) ($i = 1$, 2 and 3) we have

$$\bar{k}_{mi} = \frac{(k_{mi}(1+v_0)\bar{v}_0)}{((1+\bar{v}_0)v_0)}. \tag{19}$$

Using (19) and applying the 2nd derivative ($k = 2$) yields:

$$\bar{k}_{mo} = \frac{k_i(\bar{v}_0 - v_0)}{\bar{v}_0(1+v_0)} + \frac{v_0(k_{mi}+k_{mo}) + \bar{v}_0(k_{mo}v_0 - k_{mi})}{v_0(1+\bar{v}_0)},\ \text{and}\ \bar{k}_i = \frac{k_i v_0(1+\bar{v}_0)}{(1+v_0)\bar{v}_0}. \tag{20}$$

Now considering the next derivative ($k = 3$) in addition to using the relations in (19) and (20), the following equation must hold to satisfy (18) for each i and $k = 0, \ldots, 3$:

$$\bar{B}_T = \frac{B_T k_b}{\bar{k}_b}, \bar{k}_e = k_e, \bar{k}_i = k_i, \bar{k}_{mi} = k_{mi}, \bar{k}_{mo} = k_{mo},\ \text{and}\ \bar{v}_0 = v_0. \tag{21}$$

Calculating the fourth derivative terms ($k = 4$) and using the relations in (21), yields

$$\begin{aligned} &\bar{k}_{dl} = k_{dh} - \bar{k}_{dh} + k_{dl} + \frac{V_{m2}}{k_{m2}} - \frac{\bar{V}_{m2}}{\bar{k}_{m2}}, \\ &\text{and}\ \bar{V}_{m1} = \frac{\bar{k}_{m1}k_{m2}\bar{k}_{m2}k_{oc}V_{m1} - k_e k_{m1}\bar{k}_{m1}\bar{k}_{m2}V_{m2} + \bar{k}_{m1}\bar{k}_{m2}V_{m1}V_{m2} + k_e k_{m1}\bar{k}_{m1}k_{m2}\bar{V}_{m2}}{k_{m1}k_{m2}\bar{k}_{m2}k_{oc} + k_{m1}k_{m2}\bar{V}_{m2}}. \end{aligned} \tag{22}$$

From the next set of coefficients in the Taylor series expansions ($k = 5$), as well as using the relations in (21) and (22), the following relations must hold in order to satisfy (18) for each i and $k = 0, \ldots, 5$:

$$\begin{aligned} &\bar{B}_T = \frac{B_T k_b}{\bar{k}_b}, \bar{k}_e = k_e, \bar{k}_i = k_i, \bar{k}_{mi} = k_{mi}, \bar{k}_{mo} = k_{mo}, \bar{v}_0 = v_0 \\ &\bar{k}_{dl} = k_{dh} - \bar{k}_{dh} + k_{dl} + \frac{V_{m2}}{k_{m2}} - \frac{\bar{V}_{m2}}{\bar{k}_{m2}}, \\ &\text{and}\ \bar{V}_{m1} = \frac{\bar{k}_{m1}k_{m2}\bar{k}_{m2}k_{oc}V_{m1} - k_e k_{m1}\bar{k}_{m1}\bar{k}_{m2}V_{m2} + \bar{k}_{m1}\bar{k}_{m2}V_{m1}V_{m2} + k_e k_{m1}\bar{k}_{m1}k_{m2}\bar{V}_{m2}}{k_{m1}k_{m2}\bar{k}_{m2}k_{oc} + k_{m1}k_{m2}\bar{V}_{m2}}. \end{aligned} \tag{23}$$

Equating and substituting the parameter relations resulting from equating the sixth derivative ($k = 6$) in (23) gives

$$\begin{aligned} &\bar{B}_T = B_T, \bar{k}_b = k_b, \bar{k}_{dh} = k_{dh}, \bar{k}_{dl} = k_{dl}, \bar{V}_{m1} = \frac{\bar{k}_{m1} V_{m1}}{k_{m1}}, \bar{k}_e = k_e, \\ &\bar{k}_i = k_i, \bar{k}_{m2} = k_{m2}, \bar{k}_{mi} = k_{mi}, \bar{k}_{mo} = k_{mo}, \bar{v}_0 = v_0, \text{ and } \bar{V}_{m2} = V_{m2}. \end{aligned} \tag{24}$$

Finally, equating the eighth set of coefficients ($k = 7$), and using the relations in (24) yields

$$\begin{aligned} &\bar{B}_T = B_T, \bar{k}_b = k_b, \bar{k}_{dh} = k_{dh}, \bar{k}_{dl} = k_{dl}, \bar{k}_e = k_e, \bar{k}_i = k_i, \bar{k}_{m2} = k_{m2}, \\ &\bar{k}_{m1} = k_{m1}, \bar{k}_{mi} = k_{mi}, \bar{k}_{mo} = k_{mo}, \bar{v}_0 = v_0, \bar{V}_{m2} = V_{m2}, \text{ and } \bar{V}_{m1} = V_{m1}. \end{aligned} \tag{25}$$

Equation (18) is therefore satisfied, that is $\mathbf{p} = \bar{\mathbf{p}}$ (for each i and all k). This is true for generic $\mathbf{p} \in \Omega$, thus the model is structurally globally identifiable, that is all of the model parameters are uniquely determined by the output structure corresponding to the proposed experiments.

5. Parameter estimation

TPT uptake into each cellular compartment was screened using two photon laser scanning microscopy. The set up of the instrument was calibrated in order that the fluorescence response was linear for 0-15 μM TPT, therefore, making the conversion to the concentration of drug from fluorescence intensity (following background subtraction) simple to calculate [1].

Parameter estimation was performed using the commercial simulation software package FACSIMILE (MCPA Software, U.K.). This software uses a robust implicit numerical integrator. The optimisation method used to obtain parameter estimates involves the minimisation of the weighted least-squares criterion given by:

$$\mathbf{RSS} = \sum_{i=1}^{r} \sum_{j=1}^{N} (d_i(j) - y_i(t_j))^2 / \sigma^2{}_i \tag{26}$$

where $y_i(t_j)$ is the ith output of the model at the jth sampling time (t_j) and the corresponding experimental data point is denoted by $d_i(j)$. The dynamic fluorescent intensities representing the drug concentration were derived from the three main cell compartments: the nucleus, cytoplasm and medium. Experimental data points were collected starting from $t_1 = 0$ second to $t_{91} = 450$ seconds.

Therefore, each cell has three observations at each sampling time t_j. The standard error associated with the data series $d_i = (d_i(1),\ldots, d_i(N))$ is denoted by σ_i [35]. The standard error (σ_i) in FACSIMILE is equal to the product of e (estimate of the overall accuracy of the data) and R_i (range for the experimental data point), i.e., $\sigma_i = eR_i$.

The method that FACSIMILE uses in estimating parameters involves the natural logarithms of the model parameters. During the fitting procedure, a statistical analysis is performed to detect parameters that are not well-determined (NWD) by the data. Once detected, NWD parameters are treated as unknowns in subsequent tests. The default standard deviation of the natural logarithm (SDLN) of each of the remaining fitted parameters, $\mathbf{P}^0$, is estimated from the variance-covariance matrix of $\mathbf{P} - \mathbf{P}^0$ [1]. The 5% and 95% confidence limits are estimated for each of the well-determined parameters, assuming a normal distribution for the natural logarithms of these parameters.

Three different types of curve fittings were conducted for the model represented in (1)-(13) at pH = 7.2. Firstly, data from 13 individual cells were averaged and the postulated model fitted to these averaged data, as shown in Fig. 2a. Secondly, the model was fitted to data from an individual high loading cell (relatively high concentration of $L_n(t)$) (Fig. 2b). Thirdly, data from an individual low loading cell (relatively low concentration of $L_n(t)$) were used in the fitting (Fig. 2c). The chosen value of pH was 7.2 for the three fittings, i.e., averaged data fitting, high loader and low loader. The fitted (estimated) parameter values with estimates for their confidences are presented in Tables 1-3, where it is seen that all parameters are well-determined by the data. These parameter estimates correspond to the averaged data fitting, high loader fitting and low loader fitting respectively. The model fits in Fig. 2 show that there is close reproduction of the experimental data by the simulated output from the model with parameters taking values from Tables 1-3.

(**Fig. 2 here**)

Based on Tables 1-3, the estimated parameters are well-determined across the three fits. Additionally, the rate constant for the efflux of $L_c(t)$ into the extracellular pool (k_e) is lower in the high loader than

the low loader, indicating that this parameter plays an important role in maintaining the drug in the nucleus. Moreover, the rate constants for the flow of both $L_e(t)$ and $L_m(t)$ into the cytoplasm and extracellular pool (respectively) are higher in the high loader suggesting that these parameters preserve the active form of drug in the cellular pool. However, the binding constant (k_b) at which TPT-L binds to DNA increases for the high loader, which offers another reason why the cells receive more pharmacologically active drug. The binding affinity of the drug (k_{m1}) to the efflux pump is around 750 times higher in the low loading cells, therefore, the drug transporter mainly resists the anti-cancer agent TPT. The rate constant for dissociation of bound drug (k_{dl}) is relatively low for the high loading cell, providing another reason for the retention of the active form of the drug bound to DNA for these cells.

Although the concentration of TPT-L in the nucleus for the high loader is relatively high compared to that for the low loader, the value of B_T in the low loading cell is approximately 35 times larger. This suggests that the efflux pumping mechanism plays a key role in the resistance of anti-cancer drugs.

(**Table 1 here**)

(**Table 2 here**)

(**Table 3 here**)

Fig. 3 shows normal probability plots of the three fittings, i.e. average, high loader and low loader, and this is used to test whether or not the weighted residuals are normally distributed with standard deviation of 1 and zero mean. To obtain these normal probability plots [36]; the residuals are listed in an ascending numerical order $r_1 < r_2 < \cdots < r_{273}$ (the smallest value is numbered 1 and the largest is numbered 273), and $z_i = (i - 0.5)/273$ where ($i = 1, \ldots, 273$). Next, data tables for the normal distribution are used to obtain a Z_i value from the standard normal distribution corresponding to the cumulative probability given in the previous step. Finally, the resulting graph from the Z_i values plotted

against the ordered residuals (r_i) is the normal probability plot. Fig. 3 suggests that the residuals are normally distributed (with zero mean and a standard deviation of 1) since the graph is approximately linear. This is an indicator for the appropriateness of the standard error σ_i used for each observation y_i.

(**Fig. 3 here**)

6. Conclusions

A compartmental model of the *in vitro* kinetics of the anti-cancer agent TPT has been extended from a previously published model. The postulated model takes into account the effect of ALDH enzyme and the elimination of drug from the cytoplasm via the efflux pump.

Structural identifiability, which is an *a priori* analysis for parameter estimation, was performed using the computer algebra system MATHEMATICA, this tool has proven useful for symbolic computations mainly when they become algebraically complicated. The identifiability analysis demonstrates that all of the unknown model parameters are uniquely determined by the output structure corresponding to the real experiment.

Parameter estimation was performed using the robust software package FACSIMILE. Three different curve fittings were conducted for average, low loading and high loading cells. Model simulations have been compared with live human breast cancer cell (MCF-7 cell line) data and found to give good qualitative agreement. All unknown model parameters were estimated to a high level of confidence. In comparison between the three curve fittings, the averaged data from the 13 individual cells, the high loading cell and the low loading cell, the efflux pumping mechanism resulting from BCRP/ABCG2 transporter is a key factor in resisting the anti-cancer agent TPT. According to the normal probability plots for the weighted residuals for each of the three curve fittings, it is suggested that the weighted residuals in the three cases are normally distributed with zero mean and standard deviation of 1 indicating the appropriateness of the constant standard errors used for each observation.

The model allows *in silico* estimations and predictions of the relationship between the target binding and the dose, with different expressions of the drug resistance protein and the ALDH enzyme, leading

to the possibility of the design of optimal dosing regimens. The next step is to use the extended single-cell model in this paper to consider compartmental modelling for a population of cells and compare it to the multi-cell model described in Cheung et al. [37], to determine sensitivity, model robustness and model validation. Moreover, the current kinetics model will be coupled with a dynamics model to study the response of the regulatory protein cyclin B with the presence of the anti-cancer agent TPT to assist in drug design.

Acknowledgement

M.I. Atari gratefully acknowledges the support of the University of Warwick Vice Chancellor's Ph.D. Scholarship.

References

[1] N.D. Evans, R.J. Errington, M.J. Chapman, P.J. Smith, M.J. Chappell, K.R. Godfrey, Compartmental modelling of the uptake kinetics of the anti-cancer agent topotecan in human breast cancer cells, Int. J. Adapt. Control and Signal Process. 19 (2005) 395-417.

[2] S. Wolfram, The Mathematica Book (4th edn). Mathematica Version 4, Wolfram Media/Cambridge University Press, Cambridge, UK, 1999.

[3] C. Bailly, Topoisomerase I poisons and suppressors as anticancer drugs, Curr. Med. Chem. 7 (2000) 39-58.

[4] R. Garcia-Carbonero, J.G. Supko, Current perspectives on the clinical experience, pharmacology, and continued development of the camptothecins, Clin. Cancer Res. 8 (2002) 641-661.

[5] J. O'Leary, F.M. Muggia, Camptothecins: a review of their development and schedules of administration, Eur. J. Cancer 34 (1998) 1500-1508.

[6] Y.-H. Hsiang, L.F. Liu, Identification of mammalian DNA topoisomerase I as an intracellular target of the anticancer drug camptothecin, Cancer Res. 48 (1988) 1722-1726.

[7] J.C. Wang, DNA topoisomerases, Annu. Rev. Biochem. 65 (1996) 635-692.

[8] I. Gryczynski, Z. Gryczynski, J.R. Lakowicz, D.Z. Yang, T.G. Burke, Fluorescence spectral properties of the anticancer drug topotecan by steady-state and frequency domain fluorometry with one-photon and multi-photon excitation, Photochem. Photobiol. 69 (1999) 421-428.

[9] S. Yao, D. Murali, P. Seetharamulu, K. Haridas, P.N.V. Petluru, D.G. Reddy, F.H. Hausheer, Topotecan lactone selectively binds to double- and single-stranded DNA in the absence of topoisomerase I, Cancer Res. 58 (1998) 3782-3786.

[10] N.D. Evans, R.J. Errington, M. Shelley, G.P. Feeney, M.J. Chapman, K.R. Godfrey, P.J. Smith, M.J. Chappell, A mathematical model for the in vitro kinetics of the anti-cancer agent topotecan, Math. Biosci. 189 (2004) 185-217.

[11] Q.C. Mao, J.D. Unadkat, Role of the breast cancer resistance protein (ABCG2) in drug transport, AAPS J. 7 (2005) E118-E133.

[12] S.V. Ambudkar, C. Kimchi-Sarfaty, Z.E. Sauna, M.M. Gottesman, P-glycoprotein: from genomics to mechanism, Oncogene 22 (2003) 7468-7485.

[13] A. Haimeur, G. Conseil, R.G. Deeley, S.P. Cole, The MRP-related and BCRP/ABCG2 multidrug resistance proteins: biology, substrate specificity and regulation, Curr. Drug Metab. 5 (2004) 21-53.

[14] L.A. Doyle, W. Yang, L.V. Abruzzo, T. Krogmann, Y. Gao, A.K. Rishi, D.D. Ross, A multidrug resistance transporter from human MCF-7 breast cancer cells, Proc. Natl. Acad. Sci. USA 95 (1998) 15665-15670.

[15] R. Allikmets, L.M. Schriml, A. Hutchinson, V. Romano-Spica, M. Dean, A human placenta-specific ATP-binding cassette gene (ABCP) on chromosome 4q22 that is involved in multidrug resistance, Cancer Res. 58 (1998) 5337-5339.

[16] K. Miyake, L. Mickley, T. Litman, Z.R. Zhan, R. Robey, B. Cristensen, M. Brangi, L. Greenberger, M. Dean, T. Fojo, S.E. Bates, Molecular cloning of cDNAs which are highly overexpressed in mitoxantrone-resistant cells: demonstration of homology to ABC transport genes, Cancer Res. 59 (1999) 8-13.

[17] J.D. Allen, A.H. Schinkel, Multidrug resistance and pharmacological protection mediated by the breast cancer resistance protein (BCRP/ABCG2), Mol. Cancer Ther. 1 (2002) 427-434.

[18] S.E. Bates, R. Robey, K. Miyake, K. Rao, D.D. Ross, T. Litman, The role of half-transporters in multidrug resistance, J. Bioenerg. Biomembr. 33 (2001) 503-511.

[19] L.A. Doyle, D.D. Ross, Multidrug resistance mediated by the breast cancer resistance protein BCRP (ABCG2), Oncogene 22 (2003) 7340-7358.

[20] M. Maliepaard, G.L. Scheffer, I.F. Faneyte, M.A. van Gastelen, A.C.L.M. Pijnenborg, A.H. Schinkel, M.J. van de Vijver, R.J. Scheper, J.H.M. Schellens, Subcellular localization and distribution of the breast cancer resistance protein transporter in normal human tissues, Cancer Res. 61 (2001) 3458-3464.

[21] G.L. Scheffer, M. Maliepaard, A.C.L.M. Pijnenborg, M.A. van Gastelen, M.C. de Jong, A.B. Schroeijers, D.M. van der Kolk, J.D. Allen, D.D. Ross, P. van der Valk, W.S. Dalton, J.H.M.

Schellens, R.J. Scheper, Breast cancer resistance protein is localized at the plasma membrane in mitoxantrone- and topotecan-resistant cell lines, Cancer Res. 60 (2000) 2589-2593.

[22] A. Yoshida, A. Rzhetsky, L.C. Hsu, C. Chang, Human aldehyde dehydrogenase gene family, Eur. J. Biochem. 251 (1998) 549-557.

[23] R.A. Deltrich, Tissue and subcellular distribution of mammalian aldehyde-oxidizing capacity, Biochem. Pharmacol. 15 (1966) 1911-1922.

[24] A. Yoshida, V. Davé, H. Han, K.J. Scanlon, Enhanced transcription of the cytosolic ALDH gene in cyclophosphamide resistant human carcinoma cells, Adv. Exp. Med. Biol. 328 (1993) 63-72.

[25] J.S. Moreb, H.V. Baker, L.-J. Chang, M. Amaya, M.C. Lopez, B. Ostmark, W. Chou, ALDH isozymes downregulation affects cell growth, cell motility and gene expression in lung cancer cells, Mol. Cancer 7 (2008), DOI:10.1186/1476-4598-7-87.

[26] J.E. Visvader, G.J. Lindeman, Cancer stem cells in solid tumours: accumulating evidence and unresolved questions, Nat. Rev. Cancer 8 (2008) 755-768.

[27] P.J. Smith, E. Furon, M. Wiltshire, L. Campbell, G.P. Feeney, R.D. Snyder, R.J. Errington, ABCG2-associated resistance to Hoechst 33342 and topotecan in a murine cell model with constitutive expression of side population characteristics, Cytom. Part A 75A (2009) 924-933.

[28] S.A. Streltsov, Action models for the antitumor drug camptothecin: formation of alkali-labile complex with DNA and inhibition of human DNA topoisomerase I, J. Biomol. Struct. Dyn. 20 (2002) 447-454.

[29] A. Chen, V.T. Moy, Cross-linking of cell surface receptors enhances cooperativity of molecular adhesion, Biophys. J. 78 (2000) 2814-2820.

[30] F.G. Heineken, H.M. Tsuchiya, R. Aris, On the mathematical status of the pseudo-steady state hypothesis of biochemical kinetics, Math. Biosci. 1 (1967) 95-113.

[31] M.J. Chappell, Structural identifiability of models characterizing saturable binding: comparison of pseudo-steady-state and non-pseudo-steady-state model formulations, Math. Biosci. 133 (1996) 1-20.

[32] H. Lineweaver, D. Burk, The determination of enzyme dissociation constants, J. Am. Chem. Soc. 56 (1934) 658-666.

[33] J.A. Jacquez, Compartmental Analysis in Biology and Medicine (3rd edn), BioMedware, Ann Arbor, MI, USA, 1996.

[34] H. Pohjanpalo, System identifiability based on the power series expansion of the solution, Math. Biosci. 41 (1978) 21-33.

[35] AEA Technology Harwell Laboratory, Facsimile (Version 4.0) Technical Reference Manual, Didcot, Oxfordshire, UK, 1995.

[36] D.C. Montgomery, G.C. Runger, Applied Statistics and Probability for Engineers (4th edn), John Wiley & Sons, Inc., Hoboken, NJ, USA, 2007.

[37] S.Y.A. Cheung, N.D. Evans, M.J. Chappell, K.R. Godfrey, P.J. Smith, R.J. Errington, Exploration of the intercellular heterogeneity of topotecan uptake into human breast cancer cells through compartmental modelling, Math. Biosci. 213 (2008) 119-134.

Appendix

ALDH	Aldehyde dehydrogenase
BCRP	Breast cancer resistance protein
CPT	Camptothecin
DNA	Deoxyribonucleic acid
dsDNA	double-stranded DNA
HPLC	High performance liquid chromatography
MRP1	Multidrug resistance protein 1
NWD	Not well-determined
P-gp	P-glycoprotein
SD	Standard deviation
SDLN	Standard deviation of the natural logarithm
TPT	Topotecan
TPT-H	Topotecan hydroxy acid form
TPT-L	Topotecan lactone form

Captions

Table 1 - Parameter values for averaged data obtained for the model (1)-(13), estimated using two-photon scanning laser microscopy data. The cellular hydrolysis rate constants are fixed at values obtained from Reference [9] for pH = 7.2 buffered solution where: $k_{om} = k_{oc} = 1.5599 \times 10^{-4}\ s^{-1}$ and $k_{cm} = k_{cc} = 2.9553 \times 10^{-4}\ s^{-1}$.

Table 2 - Parameter values for high loading cell obtained for the model (1)-(13), estimated using two-photon scanning laser microscopy data. The cellular hydrolysis rate constants are fixed at values obtained from Reference [9] for pH = 7.2 buffered solution where: $k_{om} = k_{oc} = 1.5599 \times 10^{-4}\ s^{-1}$ and $k_{cm} = k_{cc} = 2.9553 \times 10^{-4}\ s^{-1}$.

Table 3 - Parameter values for low loading cell obtained for the model (1)-(13), estimated using two-photon scanning laser microscopy data. The cellular hydrolysis rate constants are fixed at values obtained from Reference [9] for pH = 7.2 buffered solution where: $k_{om} = k_{oc} = 1.5599 \times 10^{-4}\ s^{-1}$ and $k_{cm} = k_{cc} = 2.9553 \times 10^{-4}\ s^{-1}$.

Fig. 1 - Schematic of the mathematical model used to investigate the uptake kinetics of TPT in a culture medium containing human breast cancer cells (MCF-7 cell line) in suspension.

Fig. 2 - Simulated output from the model (1) – (13) with parameters taking values in Tables 1-3. (a) Average fitting (b) High loading cell. (c) Low loading cell.

Fig. 3 – Normal probability plot. (a) Average fitting (b) High loading cell. (c) Low loading cell.

Table 1

Parameter	Value	SDLN	5%	95%
k_i (s^{-1})	2.4100×10^{-2}	0.0242	2.3158×10^{-2}	2.5081×10^{-2}
k_e (s^{-1})	8.6475×10^{-3}	0.0498	7.9669×10^{-3}	9.3862×10^{-3}
k_b (s^{-1} μM^{-1})	3.2780×10^{-5}	0.0421	3.0584×10^{-5}	3.5133×10^{-5}
k_{mi} (s^{-1})	1.4630×10^{-6}	0.0267	1.4000×10^{-6}	1.5288×10^{-6}
k_{mo} (s^{-1})	9.0270×10^{-2}	0.0296	8.5983×10^{-2}	9.4770×10^{-2}
k_{dl} (s^{-1})	7.0520×10^{-2}	0.0003	7.0480×10^{-2}	7.0560×10^{-2}
k_{dh} (s^{-1})	2.8800×10^{-4}	0.0349	2.7194×10^{-4}	3.0501×10^{-4}
v_0	1.5013×10^{-5}	0.0252	1.4404×10^{-5}	1.5648×10^{-5}
B_T (μM)	$1.1734\times10^{+3}$	0.0431	$1.0932\times10^{+3}$	$1.2595\times10^{+3}$
V_{m1} (s^{-1} μM)	1.5840×10^{-4}	0.1202	1.2999×10^{-4}	1.9302×10^{-4}
V_{m2} (s^{-1} μM)	1.1500×10^{-4}	0.0629	1.0369×10^{-4}	1.2754×10^{-4}
k_{m1} (μM)	6.9740×10^{-6}	0.1167	5.7555×10^{-6}	8.4504×10^{-6}
k_{m2} (μM)	1.0555×10^{-5}	0.0456	9.7923×10^{-6}	1.1377×10^{-5}

Table 2

Parameter	Value	SDLN	5%	95%
k_i (s^{-1})	2.6069×10^{-2}	0.0621	2.3537×10^{-2}	2.8873×10^{-2}
k_e (s^{-1})	7.1650×10^{-3}	0.0502	6.5970×10^{-3}	7.7819×10^{-3}
k_b (s^{-1} μM^{-1})	9.5340×10^{-5}	0.1477	7.4777×10^{-5}	1.2156×10^{-4}
k_{mi} (s^{-1})	1.5953×10^{-6}	0.0647	1.4343×10^{-6}	1.7744×10^{-6}
k_{mo} (s^{-1})	9.0229×10^{-2}	0.0314	8.5688×10^{-2}	9.5010×10^{-2}
k_{dl} (s^{-1})	5.0529×10^{-2}	0.1230	4.1271×10^{-2}	6.1863×10^{-2}
k_{dh} (s^{-1})	4.7387×10^{-4}	0.1707	3.5785×10^{-4}	6.2750×10^{-4}
v_0	1.6083×10^{-5}	0.0698	1.4339×10^{-5}	1.8040×10^{-5}
B_T (μM)	$3.2164\times10^{+2}$	0.1713	$2.4266\times10^{+2}$	$4.2631\times10^{+2}$
V_{m1} (s^{-1} μM)	6.6807×10^{-4}	0.0593	6.0600×10^{-4}	7.3650×10^{-4}
V_{m2} (s^{-1} μM)	1.6544×10^{-4}	0.1710	1.2488×10^{-4}	2.1916×10^{-4}
k_{m1} (μM)	3.6853×10^{-3}	0.0673	3.2992×10^{-3}	4.1167×10^{-3}
k_{m2} (μM)	8.1485×10^{-6}	0.1876	5.9847×10^{-6}	1.1095×10^{-5}

Table 3

Parameter	Value	SDLN	5%	95%
k_i (s^{-1})	2.3087×10^{-2}	0.0419	2.1549×10^{-2}	2.4734×10^{-2}
k_e (s^{-1})	7.4253×10^{-3}	0.0321	7.0432×10^{-3}	7.8282×10^{-3}
k_b (s^{-1} μM^{-1})	7.4016×10^{-6}	0.0602	6.7034×10^{-6}	8.1725×10^{-6}
k_{mi} (s^{-1})	8.1920×10^{-7}	0.0295	7.8046×10^{-7}	8.5987×10^{-7}
k_{mo} (s^{-1})	8.1728×10^{-2}	0.0315	7.7595×10^{-2}	8.6081×10^{-2}
k_{dl} (s^{-1})	1.7341×10^{-1}	0.0675	1.5520×10^{-1}	1.9376×10^{-1}
k_{dh} (s^{-1})	3.8292×10^{-4}	0.0978	3.2602×10^{-4}	4.4976×10^{-4}
v_0	9.0944×10^{-6}	0.0444	8.4540×10^{-6}	9.7833×10^{-6}
B_T (μM)	$1.1815\times10^{+4}$	0.0510	$1.0864\times10^{+4}$	$1.2849\times10^{+4}$
V_{m1} (s^{-1} μM)	1.2555×10^{-4}	0.0481	1.1600×10^{-4}	1.3589×10^{-4}
V_{m2} (s^{-1} μM)	9.3606×10^{-5}	0.1076	7.8421×10^{-5}	1.1173×10^{-4}
k_{m1} (μM)	4.8979×10^{-6}	0.1119	4.0746×10^{-6}	5.8876×10^{-6}
k_{m2} (μM)	1.0419×10^{-5}	0.0591	9.4537×10^{-6}	1.1483×10^{-5}

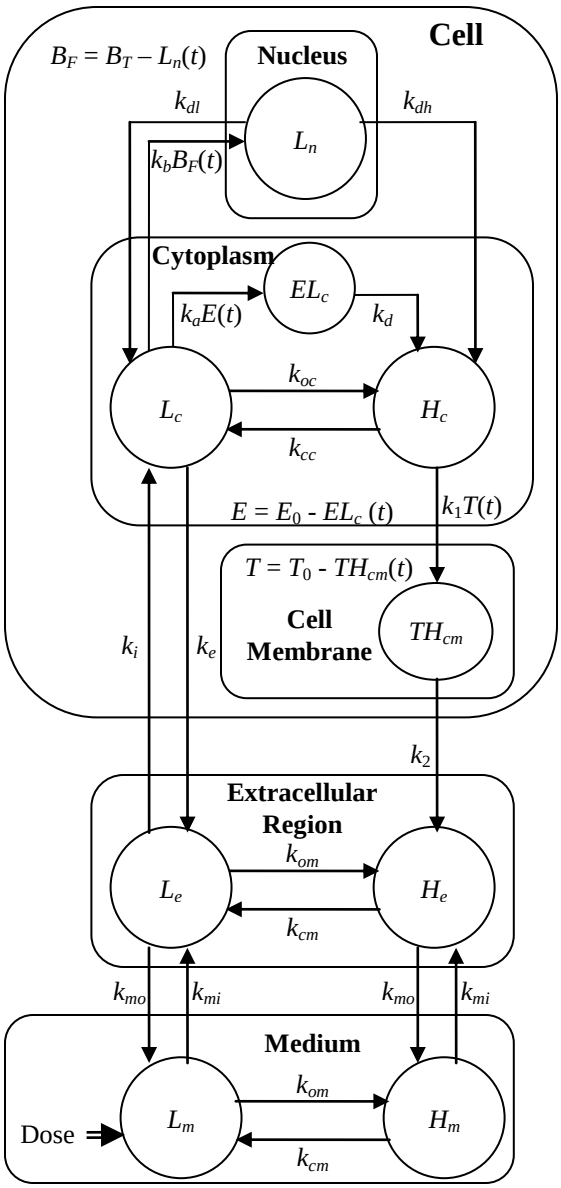
Cell
$B_F = B_T - L_n(t)$
Nucleus
k_{dl}
k_{dh}
L_n
$k_b B_F(t)$
Cytoplasm
EL_c
$k_a E(t)$
k_d
k_{oc}
L_c
H_c
k_{cc}
$E = E_0 - EL_c(t)$
$k_1 T(t)$
$T = T_0 - TH_{cm}(t)$
Cell Membrane
TH_{cm}
k_i
k_e
k_2
Extracellular Region
k_{om}
L_e
H_e
k_{cm}
k_{mo}
k_{mi}
k_{mo}
k_{mi}
Medium
k_{om}
Dose
L_m
H_m
k_{cm}

Fig. 1

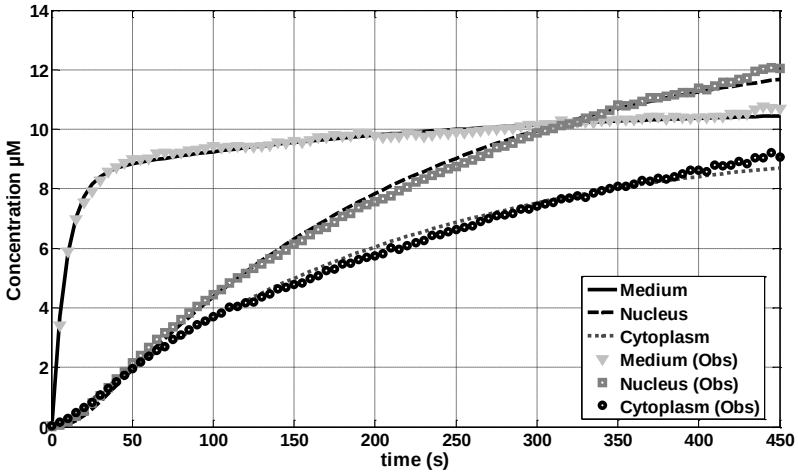
Concentration µM
time (s)
Medium
Nucleus
Cytoplasm
Medium (Obs)
Nucleus (Obs)
Cytoplasm (Obs)

(a)

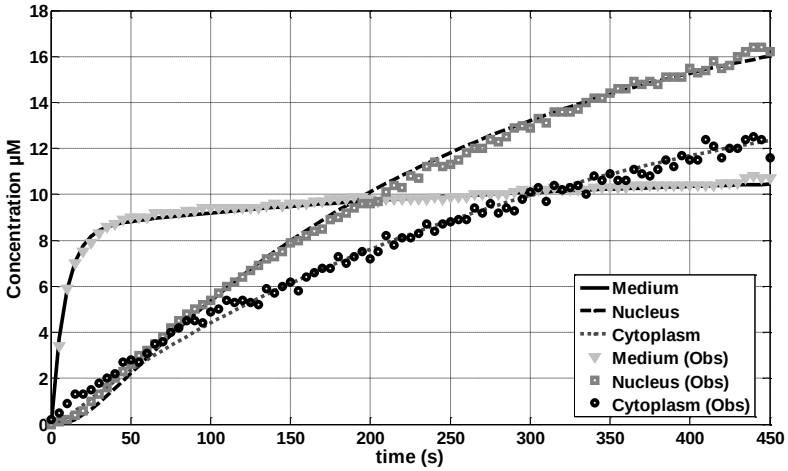
Concentration µM
time (s)
Medium
Nucleus
Cytoplasm
Medium (Obs)
Nucleus (Obs)
Cytoplasm (Obs)

(b)

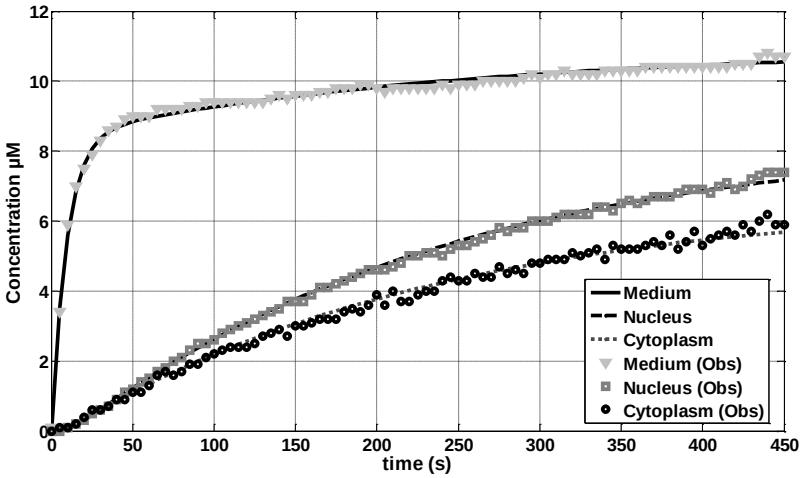
Concentration µM
time (s)
Medium
Nucleus
Cytoplasm
Medium (Obs)
Nucleus (Obs)
Cytoplasm (Obs)

(c)

Fig. 2

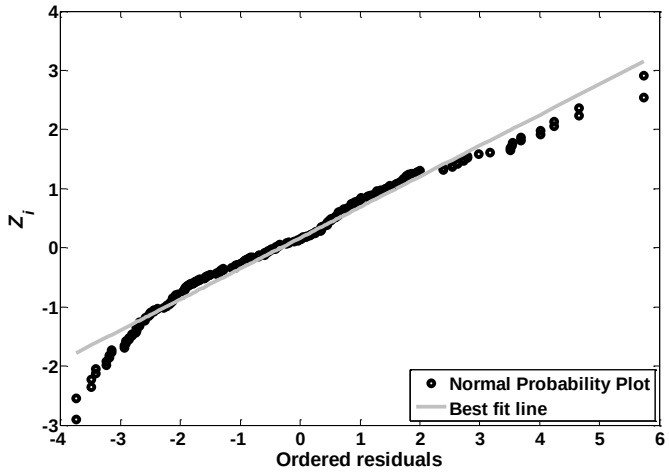
Normal Probability Plot
Best fit line
Ordered residuals
z_i

(a)

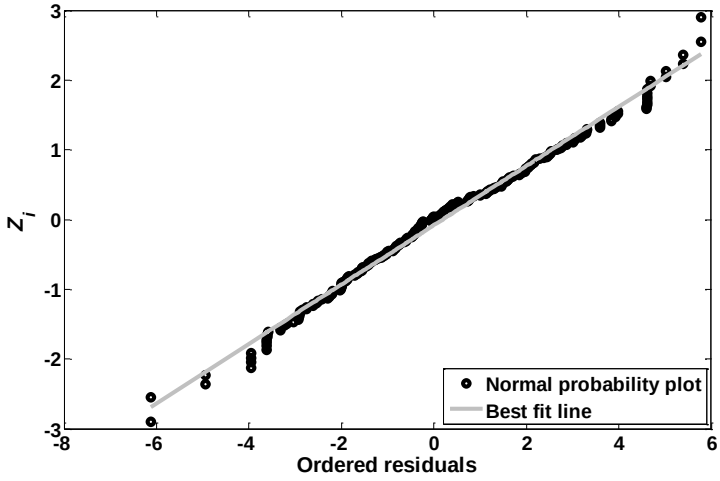
Normal probability plot
Best fit line
Ordered residuals
z_i

(b)

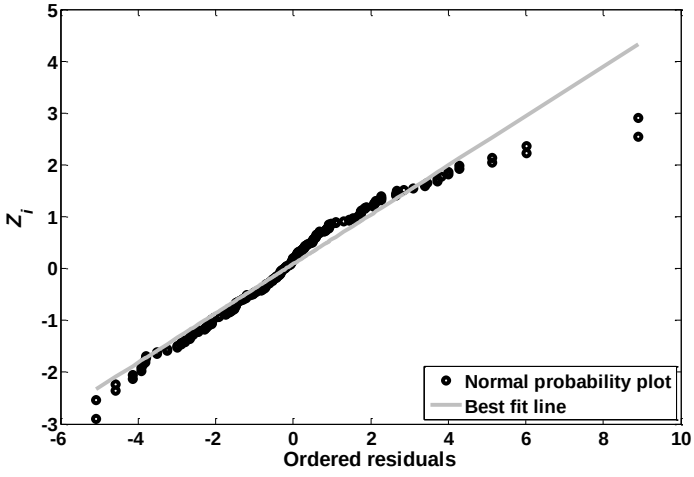
Normal probability plot
Best fit line
Ordered residuals
z_i

(c)

Fig. 3